THE JOURNAL OF PHYSICAL CHEMISTRY C

pubs.acs.org/JPCC

Article

Modification of Surface States of Hematite-Based Photoanodes by Submonolayer of TiO_2 for Enhanced Solar Water Splitting

Lauri Palmolahti, Harri Ali-Löytty, Ramsha Khan, Jesse Saari, Nikolai V. Tkachenko, and Mika Valden*

Cite This: *J. Phys. Chem. C* 2020, 124, 13094−13101

Read Online

ACCESS | Metrics & More | Article Recommendations | Supporting Information

ABSTRACT: Surface states are inherently involved with photoelectrochemical (PEC) solar fuel production; some of them are beneficial and participate in the surface reactions, but some act as recombination centers and therefore limit the PEC efficiency. Surface treatments have been applied to modify the surface states, but interrelated effects of the treatments on both types of surface states have not been properly considered. This research examines the modification of the surface states on hematite-based photoanodes by atomic layer deposition of submonolayer amount of TiO_2 and by postannealing treatments. Our results show that the postannealing causes diffusion of Ti deeper into the hematite surface layers, which leads to an increased saturation photocurrent and an anodic shift in the photocurrent onset potential. Without postannealing, the separate TiO_2 phase on the hematite surface results in a second intermediate surface state and delayed charge carrier dynamics, i.e., passivation of the recombination surface states. It is evident by these results that the intermediate surface states observed with impedance spectroscopy in a PEC cell are directly involved in the surface reaction and not with the recombination surface states observed with ultrafast (picoseconds−nanoseconds) transient absorption spectroscopy in air. These results open new optimization strategies to control the beneficial and detrimental surface states independently.

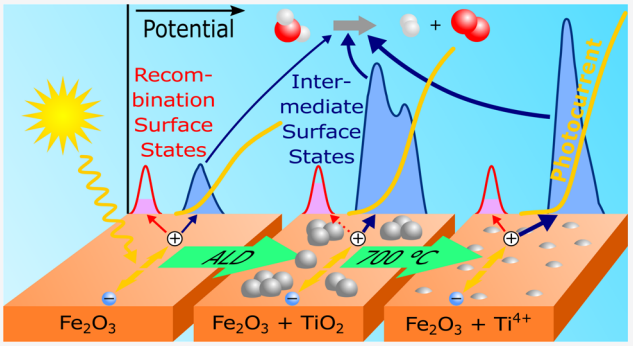

INTRODUCTION

The increased energy demand has created a need for environmentally friendly energy production methods. Solar water splitting is a method to convert solar energy into hydrogen fuel directly at the semiconductor−electrolyte interface. Hematite (α-Fe_2O_3) is a promising material for solar water splitting because it is abundant, nontoxic, and economically viable to produce. Hematite is also chemically stable in alkaline environment and has a band gap of 2.2 eV.[1] It is crucial that the band gap is large enough to produce the potential difference for the water splitting reaction (1.23 V) but small enough to be able to absorb light in the visible region.[2] Even though hematite is a promising material, it has some limitations. The charge carrier mobility is poor and the charge carrier recombination rate is high, especially at the surface states, thus limiting the overall water splitting efficiency.[3] The conduction band edge is also below the reduction potential of hydrogen, and for this reason, a bias-free hydrogen production is not possible.[4]

Surface states are electronic states that occur only at the interface between two different materials or phases. These states are due to the asymmetry of the electronic potential at the interfaces. The surface states and band structure of the hematite−electrolyte interface are illustrated in Figure 1. Two different surface states are proposed to exist: one below the conduction band and one just above the valence band. The recombination surface state (r-SS) below the conduction band is responsible for the charge carrier recombination and the intermediate surface state above the valence band (i-SS) for the hole transfer across the interface in water splitting reaction.[5,6] Electrons from the conduction band and holes from the valence band can both transfer to the r-SS. This causes the recombination of the photogenerated electron−hole pairs, thus preventing the holes from participating in the water splitting reaction at the photoanode surface. The photogenerated holes must be transferred from the valence band of the photoanode to the water molecules through the photoanode−electrolyte interface to cause the water splitting reaction. This charge transfer can proceed via i-SS or directly from the valence band if the i-SS is completely unoccupied.[7] Surface states are reported to be a necessary intermediate step for the charge carrier transfer from the semiconductor to the electrolyte,[8,9] but the surface states are also reported to cause parasitic losses, charge carrier recombination, and charge

Received: January 29, 2020
Revised: May 20, 2020
Published: May 22, 2020

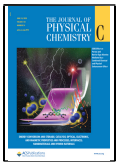

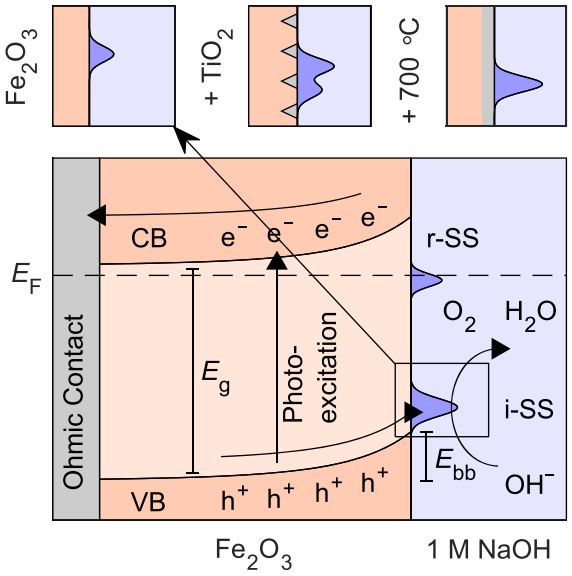

Figure 1. Schematic of the band structure of the hematite−electrolyte interface, the intermediate surface states (i-SS), the recombination surface states (r-SS), and the oxygen evolution and the charge transfer reactions during the water splitting reaction under alkaline conditions. The i-SS local density of states (LDOS) for the Fe_2O_3 and Fe_2O_3/TiO_2 samples before and after the postannealing are illustrated at the top.

carrier trapping.[10] The total effect of the surface states is thus unclear. The surface states and the charge transfer properties of the hematite−electrolyte interface can be modified by substituting a small amount of different material at the hematite surface.[3,11] To optimize the water splitting efficiency, treatments that can modify the r-SS and i-SS independently are needed. However, many of the latest publications[3,10,12] only consider passivation of the r-SS.

In this research, the effect of a submonolayer of ALD TiO_2 deposited on hematite and the effect of the postannealing at 300−700 °C on the surface states were studied with photoelectron spectroscopy, transient absorption spectroscopy, and electrochemical impedance spectroscopy. Two different surface states were identified, one of which can be directly linked with the produced photocurrent and the water splitting reaction and the other one with the charge carrier recombination.

EXPERIMENTAL SECTION

Hematite thin films were fabricated on 25 × 10 × 1.1 mm^3 indium tin oxide (ITO)-coated glass substrates (Präzisions Glas & Optik, CEC020E, ITO coating (20 ± 5 ohm/sq) coated on EAGLE2000 boro-aluminosilicate glass) by an anodic electrodeposition. The electrolyte was a 1 M solution prepared from $FeCl_2{\cdot}4H_2O$ (Sigma-Aldrich, reagent grade, ≥98%), and the temperature of the electrolyte was kept at 60 °C during the electrodeposition. The electrodeposition was done at a constant potential of +1.2 V vs Ag/AgCl electrode (Harvard Apparatus, Leak-Free reference electrode 69-0023) by using an Autolab PGSTAT101 potentiostat.[8] A charge of 60 mC/cm^2 was used in the electrodeposition, which corresponds to the film thickness of 60 nm. This was verified by XPS depth profiling shown in Figure S1. In the electrodeposition the Fe^{2+} ions oxidize and form FeOOH that was deposited on a 10 × 15 mm^2 area. FeOOH was then converted into hematite by annealing samples in a tube furnace (Carbolite Gero 30−3000 °C) at 750 °C for 8 h. The heating and cooling ramps were 5 and 1 °C/min, respectively. The formation of hematite was confirmed from the XRD patterns shown in Figure S2. In addition, the annealing induced a diffusion of In and Sn from the ITO substrate to the surface and a concurrent doping of the hematite layer with In and Sn as shown in Figure S3. This has been found to be beneficial to the photocurrent because of the increased charge carrier concentration.[13−15]

After the electrodeposition and annealing, two ALD cycles of TiO_2 were deposited on the top of the fabricated hematite films, which correspond to the average film thickness of 0.07 nm or 0.2 monolayers based on the growth per cycle determined from thicker films by ellipsometry (Rudolph Auto EL III ellipsometer, Rudolph Research Analytical). The deposition was performed at 200 °C in a Picosun Sunale ALD R200 Advanced reactor. Before starting the deposition the substrates were held in the reaction chamber for 30 min to stabilize the temperature. Tetrakis(dimethylamido)titanium-(IV) (TDMAT, electronic grade, 99.999+%, Sigma-Aldrich) and ultrapure Milli-Q water were used as precursors. During the deposition the TDMAT bubbler and the precursor gas delivery line was kept at 76 and 85 °C, respectively, to reach the proper vapor pressure and to prevent condensation of the precursor. The water was cooled to 18 °C with a Peltier element. Ar gas was used as a carrier/purge/venting gas (99.9999%, Oy AGA Ab).[16] The continuous Ar flow in the TDMAT and water lines was 100 sccm. The deposition was started with the 1.6 s TDMAT pulse and was followed by the 0.1 s water pulse. Between each pulse the excess precursor was pumped during the 6.0 s purge period.

A total of 18 samples were fabricated, from which three without TiO_2 were used as reference. The remaining 15 samples were postannealed at 300, 400, 500, 600, and 700 °C for 1 h, three samples at each temperature, to verify the reproducibility of the measurements. We note that all the samples had been subject to a heat treatment at 750 °C before the TiO_2 deposition, and therefore the diffusion of In and Sn within the bulk of the hematite and the decrease in conductivity of the ITO substrate during the postannealing are assumed negligible. Annealing at 300 °C or higher temperatures provides reasonable stability of ALD TiO_2 during chopped light measurements under the water splitting condition (Figure S4).[16]

Equipment used for XPS measurements included an analysis chamber, a load lock chamber, an X-ray source (V. G. Microtech, 8025 twin anode X-ray source), and an energy analyzer with electron multiplier and detector (V. G. Microtech, CLAM4MCD LNo5). All measurements were conducted by using X-ray source operated at 300 W power and Al anode (Al Kα, $h\nu$ = 1486.7 eV). The pressure of the analysis chamber was below 2 × 10^{-8} mbar. XP spectra were calibrated so that the binding energy of the Fe^{3+} $2p_{3/2}$ peak is at 710.6 eV.

Electrochemical impedance spectroscopy (EIS) and linear sweep voltammetry (LSV) were performed by using a three-electrode setup with an Ag/AgCl reference electrode (Harvard Apparatus, Leak-Free reference electrode 69-0023), a platinum wire counter electrode, and a sample as an working electrode (the diameter of the sample−electrolyte contact was 6 mm). The photoelectrochemical cell was filled with 3.5 mL of 1 M solution of NaOH (Sigma-Aldrich, sodium hydroxide, reagent grade) (pH 13.6). Measurements were done by an Autolab PGSTAT12 potentiostat (Metrohm AG) equipped with a

https://dx.doi.org/10.1021/acs.jpcc.0c00798
J. Phys. Chem. C 2020, 124, 13094−13101

frequency response analyzer (FRA2). The measured potential was converted to potential versus reversible hydrogen electrode (RHE) using the equation $V_{RHE} = V_{Ag/AgCl} + 0.197$ V + 0.0592 V × pH. The front side of the sample was illuminated through the electrolyte with an Asahi Spectra HAL-C100 solar simulator, and the intensity was calibrated by a 1 sun checker (Asahi Spectra CS-30).

Transient absorption spectra (TAS) of the Fe_2O_3/TiO_2 samples were measured by using a pump−probe setup with an excitation wavelength of 380 nm under ambient air conditions. The excitation density was roughly 1 $\mu J/cm^2$. The primary laser pulses were obtained by using a Ti:sapphire laser (Libra F, Coherent Inc., 100 fs pulse at 1 kHz repetition rate). Most of the laser radiation was directed to a parametric amplifier (Topas C, Light Conversion Ltd.) to generate the pump pulses. Time-resolved transient absorption spectra were recorded by using ExciPro TA spectrometer (CDP, Inc.) in the wavelength range 430−730 nm.

RESULTS AND DISCUSSION

Mixing of TiO_2 and Fe_2O_3 Layer. The effect of the postannealing on the mixing of TiO_2 and the Fe_2O_3 layer was studied by XPS. The XP spectra were measured before and after the ALD TiO_2 deposition and after the postannealing. The Fe $2p_{3/2}$ spectra were fitted with parameters described in ref 17 for hematite. The Fe $2p_{3/2}$ and Ti $2p_{3/2}$ spectra of Fe_2O_3/TiO_2 samples postannealed at 300 and 700 °C are presented in Figure 2. The binding energy of the Fe $2p_{3/2}$ peak

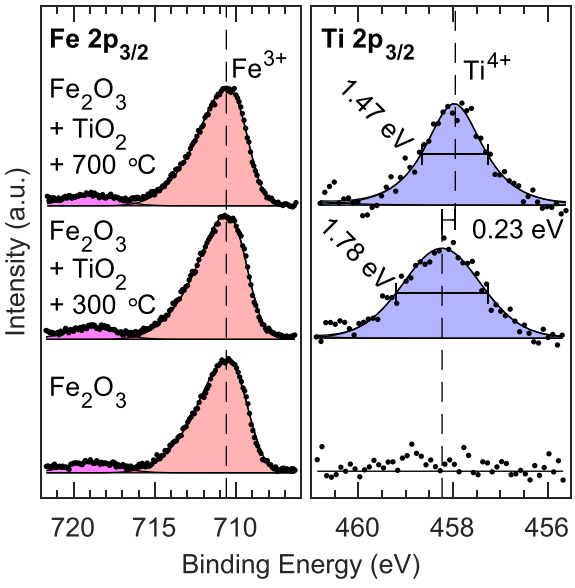

Figure 2. XP spectra of Fe_2O_3 and two Fe_2O_3 + TiO_2 samples. The Fe $2p_{3/2}$ peak (red) and the Fe $2p_{3/2}$ shakeup satellite peak (purple) are presented on the left, and the Ti $2p_{3/2}$ peak (blue) is presented on the right.

can be attributed to the oxidation state of 3+, and no changes in the Fe 2p peak shape were observed between samples. In contrast, the Ti^{4+} $2p_{3/2}$ peak shows a shift of −0.31 eV and a decrease in full width at half-maximum value from 1.78 to 1.47 eV as the postannealing temperature is increased from 300 to 700 °C. Spectra for other samples are presented in Figure S3. The relative atomic concentrations and the binding energy values for the photoemission peaks of Fe, Ti, In, and Sn were obtained from XPS results and are presented in Figure 3.

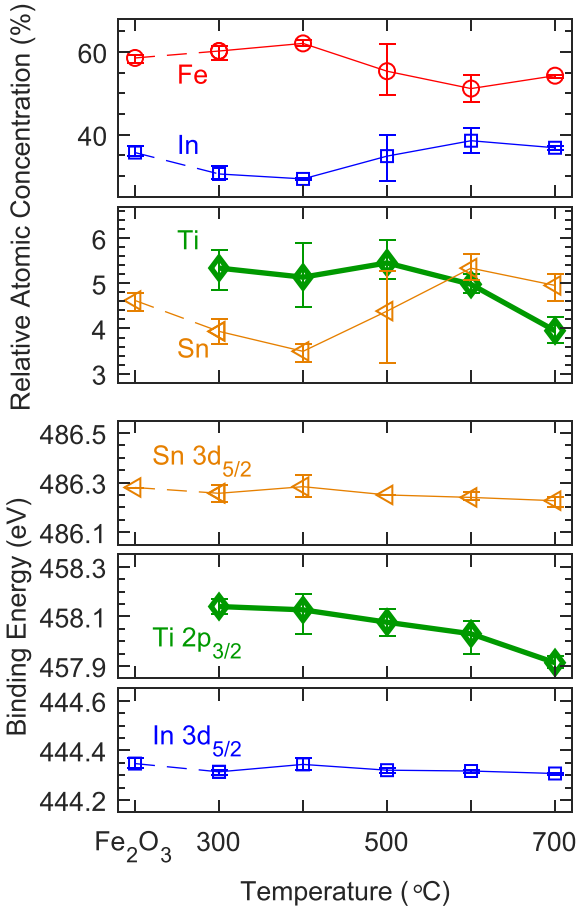

Figure 3. Relative atomic concentrations (upper) and the binding energies (lower) of Fe $2p_{3/2}$, In $3d_{5/2}$ Ti $2p_{3/2}$, and Sn $3d_{5/2}$ XPS peaks for the Fe_2O_3 sample and Fe_2O_3/TiO_2 samples annealed at temperatures ranging from 300 to 700 °C. The values are mean of three samples, and the error bars represent the range of variation. O and C are excluded because all C and large portion of O are from the air contamination. Also, a small amount of Si (<3 at. %) was detected by XPS in all the samples and in the ITO substrate before FeOOH deposition. The binding energies were calibrated so that the binding energies of Fe $2p_{3/2}$ peak components corresponded to literature values for hematite.[17] The binding energies of the Sn $3d_{5/2}$ and In $3d_{5/2}$ peaks are fairly constant. A decrease of Ti and an increase of Fe, In, and Sn indicate that the Ti at the surface mixes with Fe_2O_3 surface layer during postannealing which is further supported by the decrease of the Ti $2p_{3/2}$ binding energy.

For the postannealing temperatures higher than 500 °C the surface concentration of Ti decreases while the surface concentrations of In and Sn are increased (Figure 3). This indicates the diffusion of Ti at high temperatures from the surface into the top layer of hematite and the formation of mixed $Fe^{3+}Ti^{4+}$ surface oxide. The decreasing binding energy of the Ti $2p_{3/2}$ peak with the increasing postannealing temperature follows the same trend with the Ti concentration. According to Hiltunen et al.,[18] the binding energy of the Ti $2p_{3/2}$ peak shifts from 458.84 to 458.43 eV when Ti is mixed with Fe_2O_3. Because the peak shift is smaller than the chemical shift between Ti^{3+} and Ti^{4+},[19] there is no change in the oxidation state of Ti. The binding energies of the Sn $3d_{5/2}$ and

https://dx.doi.org/10.1021/acs.jpcc.0c00798
J. Phys. Chem. C 2020, 124, 13094−13101

In $3d_{5/2}$ do not change, which indicates that Sn and In stay in the same chemical environment (in Fe_2O_3) and that the chemical state does not change. At 700 °C the trend changes and the concentrations of In and Sn decrease slightly whereas the concentration of Fe increases.

Raman spectra showed no difference between the samples with submonolayer amount of ALD TiO_2 (two cycles) and the Fe_2O_3 reference due to the insufficient amount of TiO_2. However, an increase in LO peak (forbidden longitudinal optical mode) at 660 cm^{-1} was detected for samples with 15 ALD TiO_2 cycles when film structure was postannealed at 750 °C (Figure S5). The increase in LO peak is linked with increase in the disorder in the crystal lattice.[20] This supports the hypothesis of diffusion of Ti^{4+} into the hematite film. The structures of fabricated films were confirmed to be mesoporous by scanning electron microscopy (Figure S6). The morphology of the samples is not affected by the TiO_2 deposition or postannealing treatments.

The band gap of the Fe_2O_3/TiO_2 samples was defined by Tauc analysis (Figures S7 and S8). The indirect band gap was 2.1 eV for all samples, and neither the ALD TiO_2 deposition nor the postannealing had any effect on the band gap.

Surface States and Photocatalytic Properties. Photoelectrochemical (PEC) measurements were performed to determine the photoresponse, chemical stability, and the charge transfer properties of the Fe_2O_3/TiO_2 samples. PEC measurements included electrochemical impedance spectroscopy (EIS), linear sweep voltammetry (LSV), and chronoamperometric measurements. LSV curves are presented in Figures 4 and 7. TiO_2 addition to the hematite surface and

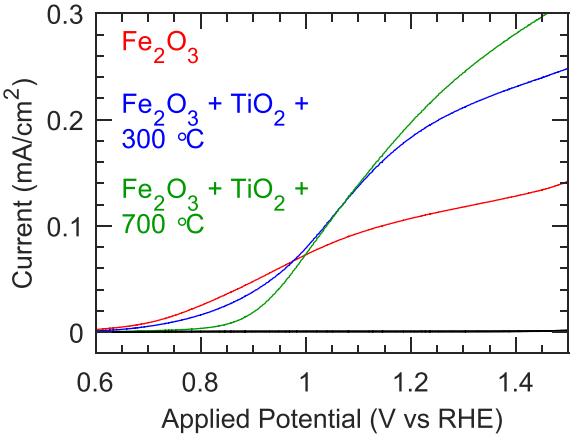

Figure 4. Linear sweep voltammetry curves for Fe_2O_3 and Fe_2O_3/TiO_2 samples annealed at 300 and 700 °C under 1 sun illumination (red, blue, and green) and in dark (black). The addition of Ti and postannealing shifts the onset potential anodically and increases the saturation photocurrent.

postannealing were found to increase the saturation photocurrent and shift the onset potential anodically. The same trend in the photocurrent density curve is reported in the literature to be resulted from the Ti doping of hematite.[21,22] In sharp contrast, effectively the same change in the saturation photocurrent resulted here from the Ti addition to the surface without doping of the hematite films, since the mixing of surface Ti with hematite is shown in Figure 3 to require temperatures higher than 500 °C. Postannealing is also reported to cause oxygen vacancies at the surface, which contributes to the doping concentration.[23]

The equivalent circuit presented in Figure 5 was used to model frequency response of the hematite−electrolyte inter-

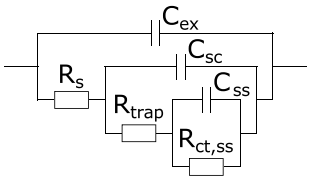

Figure 5. Equivalent circuit used to model the Fe_2O_3/TiO_2−electrolyte interface. C_{ex} is the capacitance due to the measuring arrangements, R_s is the resistance of the electrolyte, C_{sc} is the capacitance of the space charge layer of the Fe_2O_3/TiO_2−electrolyte interface, C_{ss} is capacitance of the surface states, $R_{ct,ss}$ is the charge transfer resistance, and R_{trap} is the trapping resistance of the surface states.[7]

face. A similar equivalent circuit is commonly used for fitting impedance data.[9,24−26] The circuit is the simplest equivalent circuit that can model the impedance response of the hematite−electrolyte interface with reasonable accuracy. R_s and C_{ex} were found to be constant across potential range as the external capacitance and resistance of the solution do not depend on the applied potential. The C_{sc}^{-2} vs applied potential plot is linear, which supports that the C_{sc} presents the capacitance of the semiconductor−electrolyte interface.

The flat-band potential was calculated from the EIS data by fitting the equivalent circuit (Figure 5) and doing Mott−Schottky analysis from C_{sc} component (Figure S9). Hematite is an n-type semiconductor, and a relative permittivity of 32 was used in the calculations.[9] Obtained results are shown in Figure 6. The flat-band potential of hematite before the ALD

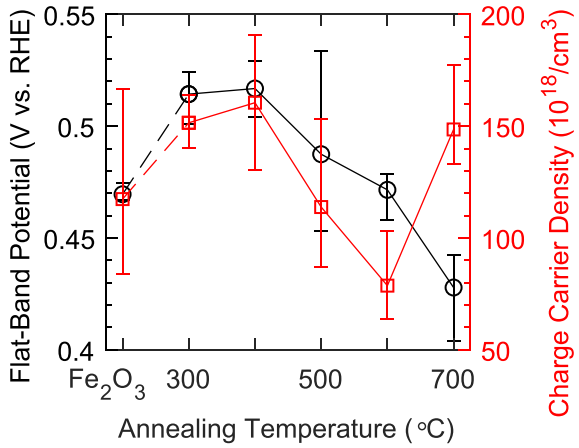

Figure 6. Flat-band potential and the charge carrier density of Fe_2O_3 and Fe_2O_3/TiO_2 samples as a function of postannealing temperature calculated from C_{sc} using Mott−Schottky analysis. Values are mean of the results measured from three samples, and error bars represent the variation between these results. A relative permittivity of 32 was used for calculations.

deposition of TiO_2 was 0.48 V vs RHE. The deposition increased and the postannealing at 400−600 °C decreased the flat-band potential. Similar flat-band potentials are reported in the literature for the hematite/1 M NaOH interface.[27] The charge carrier density followed a similar trend compared to the flat-band potential. However, the charge carrier density drastically increased when the samples were postannealed at

https://dx.doi.org/10.1021/acs.jpcc.0c00798
J. Phys. Chem. C 2020, 124, 13094−13101

700 °C. We note that the information depth of XPS analysis corresponds to the depletion region width of the Fe_2O_3 photoanodes that was 4−6 nm based on the Mott−Schottky analysis. Thus, we assign the increase in the charge carrier density at 700 °C to the increased surface concentration of Fe^{3+} shown in Figure 3.

The photocurrent onset potentials reported for hematite in the literature[5,9,28−32] show strong variation ranging typically from +0.70 to +1.15 V vs RHE, and therefore it is challenging to compare absolute values with the literature. However, our values (+0.77 to +0.89 V vs RHE) fall within the range reported in the literature, and most importantly we were able to assign the anodic shift to the change in the surface composition. Furthermore, the largest variation in all results was observed for samples postannealed at 500 °C, which corresponds to the temperature range where surface composition changes strongly

The photocurrent onset potential is directly related to the flat-band potential plus the overpotential needed to drive the water splitting reaction.[7] A more cathodic flat-band potential causes larger band bending, resulting in better charge separation and thus lower charge recombination rate.[33] The flat-band potential does not correlate with the photocurrent onset potential, which implies that the needed overpotential changes when TiO_2 is deposited on the hematite films and when films are postannealed. This anodic shift can be linked to the change in the i-SS.[34]

The LDOS of the i-SS can be determined from the surface state capacitance. The filling of the surface states at certain potential is directly proportional to the capacitance $g(E) = C/q$.[9] The surface state capacitance C_{ss} was obtained from the frequency response of the hematite−electrolyte interface (Figures S10−S21). The obtained surface state capacitance is shown in Figure 7, and the measurements were done in the dark and under 100 mW/cm^2 (1 sun) illumination with applied external bias voltage. Surface state capacitance was only observed when measurements were done under illumination. This indicates that filling or depleting of these states does not occur unless photons excite electron−hole pairs.

Two wide and low C_{ss} peaks are observed in the case of the Fe_2O_3 sample while the C_{ss} peaks are much more distinct for the Fe_2O_3/TiO_2 samples postannealed at 300 °C. Similar results are reported in the literature,[5] and it was discovered that the deposition of a different material on top of the hematite films, such as Al_2O_3, produces two distinct peaks.[5,35] Postannealing at 500 °C or higher temperatures causes the right peak to disappear and the left peak to move to the more anodic potential. The photocurrent onset is at the potential corresponding the maximum of the left C_{ss} peak, and the onset potential and peak positions change equally. The height of the peak is larger for samples postannealed at 500 °C or higher temperatures. For these samples the photocurrent onset is also sharper, and from these results it can be concluded that the left C_{ss} peak is related to the photocurrent onset potential and thus to the water splitting charge transfer reaction.[5] The i-SS can be described by Tamm states which are induced by unsaturated oxygen at the surface. These states exist just above valence band.[21,33]

The right peak does not shift but is superimposed when the postannealing temperature is higher than 500 °C. Similar double peaks were reported in the literature for Al_2O_3-coated electrodes,[5] and presumably this capacitance peak can be attributed to two different surface phases. The mixing of TiO_2 and Fe_2O_3 layers causes the peaks to combine.

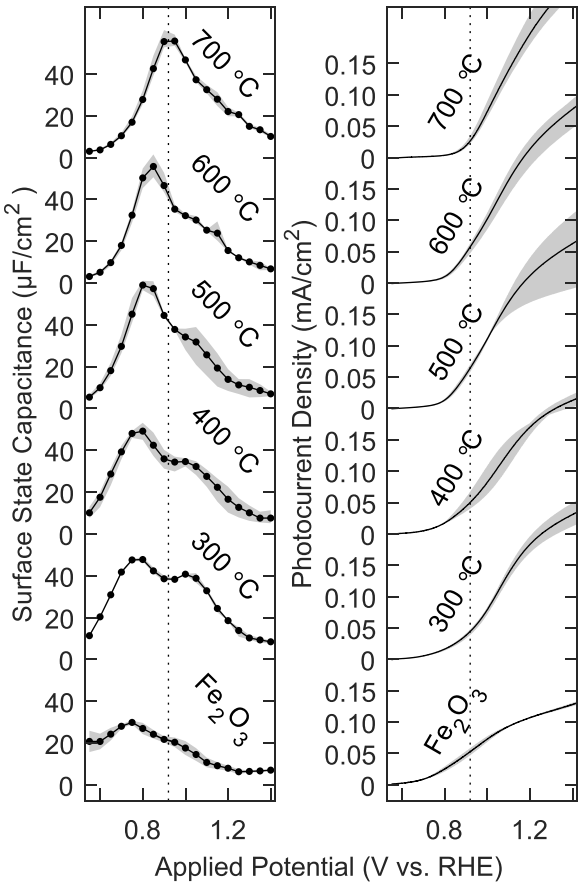

Figure 7. Surface state capacitance and photocurrent of Fe_2O_3 film and Fe_2O_3/TiO_2 films postannealed at different temperatures. The gray area indicates variation of the results measured from three samples.

The r-SS is difficult to detect by impedance spectroscopy because no charge transfer takes place through these states.[5] The r-SS was studied by TAS. The measurements were done in air without electrolyte, and therefore the data do not provide information about the i-SS. Instead, the differences in TAS spectra can be compared and be linked with the material properties of hematite. The trapping and recombination of charge carriers take place at the picoseconds−nanoseconds time scale, which is significantly faster than the charge transfer (∼1 s time scale) across the hematite−electrolyte interface.[1] The recombination dynamics in hematite probed by TAS in the microseconds−milliseconds time scale at 580 nm has been reported to be insensitive to the electrode environment.[36] For these reasons, the TAS measurements conducted in the absence of electrolyte provide here information about the charge carrier dynamics of the r-SS in the hematite films.

To compare charge carrier dynamics between the samples, the TAS spectra were normalized at a delay time of 0.2 ps (Figure 8 and Figure S22). The spectra featured a strong peak at 570 nm, which is also reported in the literature for measurements done under electrolyte conditions.[37−39] The wavelength corresponds to an electron transition of 2.1 eV from the top of the valence band to the localized states just below the conduction band.[1] The shapes of the spectra at 0.2

https://dx.doi.org/10.1021/acs.jpcc.0c00798
J. Phys. Chem. C 2020, 124, 13094−13101

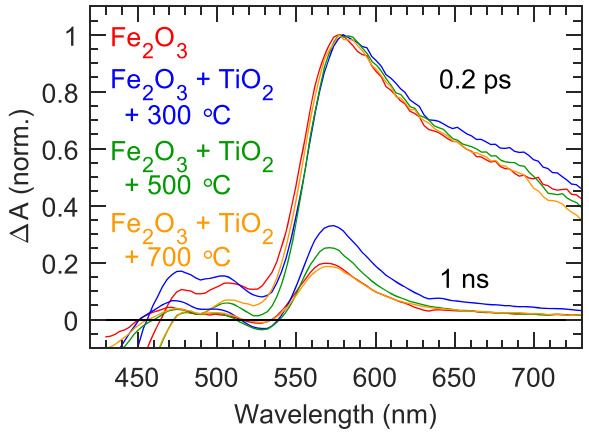

Figure 8. Transient absorption of the Fe_2O_3/TiO_2 samples at 0.2 ps and 1 ns after excitation normalized according transient absorption at 0.2 ps delay time. The red part of the spectra is almost completely decayed, which indicates the disappearance of the free charge carriers. The remaining transient absorption at 570 nm can be attributed to the charge carrier recombination and trap state population.

ps are virtually the same for all the samples, which is reasonable as at 0.2 ps delay free carriers in Fe_2O_3 dominate the transient absorption response. However, at longer delay times the spectral difference becomes more pronounced. At 570 nm the signal is on the level of 0.2−0.3 relative to that at 0.2 ps, and even stronger decay can be seen in the red side of the spectrum at wavelengths longer than 640 nm. As a rough approximation, an almost complete decay in the red part can be attributed to the disappearance of the free carriers and the remaining absorption at 570 nm to the r-SS in Fe_2O_3.[37] The sample postannealed at 300 °C shows the least degree of recombination of free carriers and the highest r-SS population at 1 ns delay time. Interestingly, the charge carrier lifetime is prolonged only when there exists a separate TiO_2 phase at the hematite surface, and the charge carrier concentration in the trap states is thus higher. From this it can be concluded that TiO_2 clearly modifies the r-SS. In general, the increased charge carrier lifetime increases the probability of the charge carriers to take part in the water splitting reaction.[32]

The TAS results confirmed the successful passivation of the r-SS by the TiO_2 phase. Strikingly, no difference in the TAS signals was observed between the sample with Ti diffused into the hematite surface and the hematite reference. This suggests that the differences in the PEC performance presented in Figure 7 are not due to the charge carrier dynamics associated with the r-SS. In contrast, these results support the hypothesis that the intermediate surface states (i-SS) probed via the surface state capacitance are involved with the charge transfer during the water splitting reaction.

CONCLUSIONS

The surface states of the hematite photoanodes take part in the charge carrier transfer, trapping, and recombination processes during the solar water splitting reaction, having a significant impact on the photocatalytic efficiency. The modification of the hematite surface states by a submonolayer of ALD TiO_2 was studied by impedance spectroscopy and transient absorption spectroscopy. The results show that the surface states are a necessary intermediate step in water splitting reaction, and the charge transfer can only take place when holes are occupying the intermediate surface states (i-SS). The potential of the i-SS affects the photocurrent onset potential, and the LDOS of i-SS affects the amount of generated photocurrent, thus corresponding to the sharpness of the photocurrent onset. Two different surface phases (Fe_2O_3 and TiO_2) give rise to two distinct surface state capacitance peaks. Postannealing causes the mixing of the layers and thus the merging of the i-SS peaks. Unfortunately, this also shifts the LDOS of the i-SS and the photocurrent onset to the anodic direction, which decreases the overall water splitting efficiency. The charge carrier lifetime in recombination surface states (r-SS) is increased when a separate TiO_2 phase exists at the hematite surface, which results in an efficient passivation of these detrimental surface states.

This work provides a deeper understanding on the type and role of surface states in photoelectrochemical water oxidation on hematite-based photoanodes. The effects of the beneficial intermediate surface states and detrimental recombination surface states to the overall water splitting efficiency seem to be uncorrelated, which opens new optimization strategies to the photoelectrode surface treatments.

ASSOCIATED CONTENT

Supporting Information

The Supporting Information is available free of charge at https://pubs.acs.org/doi/10.1021/acs.jpcc.0c00798.

Material characterization results (PDF)

AUTHOR INFORMATION

Corresponding Author

Mika Valden − *Surface Science Group, Faculty of Engineering and Natural Sciences, Tampere University, Tampere, Finland*; Email: mika.valden@tuni.fi

Authors

Lauri Palmolahti − *Surface Science Group, Faculty of Engineering and Natural Sciences, Tampere University, Tampere, Finland*; orcid.org/0000-0001-9992-6628

Harri Ali-Löytty − *Surface Science Group, Faculty of Engineering and Natural Sciences, Tampere University, Tampere, Finland*; orcid.org/0000-0001-8746-7268

Ramsha Khan − *Chemistry and Advanced Materials Group, Faculty of Engineering and Natural Sciences, Tampere University, Tampere, Finland*

Jesse Saari − *Surface Science Group, Faculty of Engineering and Natural Sciences, Tampere University, Tampere, Finland*; orcid.org/0000-0001-6741-0838

Nikolai V. Tkachenko − *Chemistry and Advanced Materials Group, Faculty of Engineering and Natural Sciences, Tampere University, Tampere, Finland*; orcid.org/0000-0002-8504-2335

Complete contact information is available at: https://pubs.acs.org/10.1021/acs.jpcc.0c00798

Notes

The authors declare no competing financial interest.

ACKNOWLEDGMENTS

This work was supported by the Academy of Finland (Decision Nos. 141481, 286713, 326406, 309920, and 326461), the Jane & Aatos Erkko Foundation (project "SOFUS"), and Business Finland (Decision No. 1464/31/

2019). L.P. was supported by the KAUTE Foundation, H.A.-L. by the Jenny and Antti Wihuri Foundation, and J.S. by the Vilho, Yrjö and Kalle Väisälä Foundation of the Finnish Academy of Science and Letters. This work is part of the Academy of Finland Flagship Programme, Photonics Research and Innovation (PREIN) (Decision No. 320165).

REFERENCES

(1) Barroso, M.; Pendlebury, S. R.; Cowan, A. J.; Durrant, J. R. Charge carrier trapping, recombination and transfer in hematite (α-Fe_2O_3) water splitting photoanodes. *Chem. Sci.* **2013**, *4*, 2724−2734.
(2) Sim, Y.; John, J.; Surendran, S.; Moon, B.; Sim, U. Efficient photoelectrochemical water splitting reaction using electrodeposited Co3Se4 catalyst. *Appl. Sci.* **2019**, *9*, 16.
(3) Hu, Z.; Shen, Z.; Yu, J. C. Covalent fixation of surface oxygen atoms on hematite photoanode for enhanced water oxidation. *Chem. Mater.* **2016**, *28*, 564−572.
(4) Pan, H.; Meng, X.; Qin, G. Hydrogen generation by water splitting on hematite (0001) surfaces: first-principles calculations. *Phys. Chem. Chem. Phys.* **2014**, *16*, 25442−25448.
(5) Wang, Z.; Fan, F.; Wang, S.; Ding, C.; Zhao, Y.; Li, C. Bridging surface states and current-potential response over hematite-based photoelectrochemical water oxidation. *RSC Adv.* **2016**, *6*, 85582−85586.
(6) Ulman, K.; Nguyen, M.-T.; Seriani, N.; Gebauer, R. Passivation of surface states of α-Fe_2O_3 (0001) surface by deposition of Ga_2O_3 overlayers: A density functional theory study. *J. Chem. Phys.* **2016**, *144*, 094701.
(7) Iandolo, B.; Hellman, A. The role of surface states in the oxygen evolution reaction on hematite. *Angew. Chem., Int. Ed.* **2014**, *53*, 13404−13408.
(8) Zandi, O.; Schon, A. R.; Hajibabaei, H.; Hamann, T. W. Enhanced charge separation and collection in high-performance electrodeposited hematite films. *Chem. Mater.* **2016**, *28*, 765−771.
(9) Klahr, B.; Gimenez, S.; Fabregat-Santiago, F.; Hamann, T.; Bisquert, J. Water oxidation at hematite photoelectrodes: the role of surface states. *J. Am. Chem. Soc.* **2012**, *134*, 4294−4302.
(10) Le Formal, F.; Tétreault, N.; Cornuz, M.; Moehl, T.; Grätzel, M.; Sivula, K. Passivating surface states on water splitting hematite photoanodes with alumina overlayers. *Chem. Sci.* **2011**, *2*, 737−743.
(11) Yang, X.; Liu, R.; Du, C.; Dai, P.; Zheng, Z.; Wang, D. Improving hematite-based photoelectrochemical water splitting with ultrathin TiO_2 by atomic layer deposition. *ACS Appl. Mater. Interfaces* **2014**, *6*, 12005−12011.
(12) Liu, R.; Zheng, Z.; Spurgeon, J.; Yang, X. Enhanced photoelectrochemical water-splitting performance of semiconductors by surface passivation layers. *Energy Environ. Sci.* **2014**, *7*, 2504−2517.
(13) Kaouk, A.; Ruoko, T.-P.; Pyeon, M.; Gönüllü, Y.; Kaunisto, K.; Lemmetyinen, H.; Mathur, S. High water-splitting efficiency through intentional In and Sn codoping in hematite photoanodes. *J. Phys. Chem. C* **2016**, *120*, 28345−28353.
(14) Ling, Y.; Wang, G.; Wheeler, D. A.; Zhang, J. Z.; Li, Y. Sn-doped hematite nanostructures for photoelectrochemical water splitting. *Nano Lett.* **2011**, *11*, 2119−2125.
(15) Hu, Y.-S.; Kleiman-Shwarsctein, A.; Forman, A. J.; Hazen, D.; Park, J.-N.; McFarland, E. W. Pt-doped α-Fe_2O_3 thin films active for photoelectrochemical water splitting. *Chem. Mater.* **2008**, *20*, 3803−3805.
(16) Ali-Löytty, H.; Hannula, M.; Saari, J.; Palmolahti, L.; Bhuskute, B. D.; Ulkuniemi, R.; Nyyssönen, T.; Lahtonen, K.; Valden, M. Diversity of TiO_2: Controlling the molecular and electronic structure of atomic-layer-deposited black TiO_2. *ACS Appl. Mater. Interfaces* **2019**, *11*, 2758−2762.
(17) Biesinger, M. C.; Payne, B. P.; Grosvenor, A. P.; Lau, L. W.; Gerson, A. R.; Smart, R. S. C. Resolving surface chemical states in XPS analysis of first row transition metals, oxides and hydroxides: Cr, Mn, Fe, Co and Ni. *Appl. Surf. Sci.* **2011**, *257*, 2717−2730.
(18) Hiltunen, A.; Ruoko, T.-P.; Iivonen, T.; Lahtonen, K.; Ali-Löytty, H.; Sarlin, E.; Valden, M.; Leskelä, M.; Tkachenko, N. Design aspects of all atomic layer deposited TiO_2-Fe_2O_3 scaffold-absorber photoanodes for water splitting. *Sustain. Energy Fuels* **2018**, *2*, 2124−2130.
(19) Moulder, J.; Chastain, J. *Handbook of X-ray Photoelectron Spectroscopy: A Reference Book of Standard Spectra for Identification and Interpretation of XPS Data*; Physical Electronics Division, Perkin-Elmer Corporation: Eden Prairie, MN, 1992.
(20) Jang, J.-W.; Du, C.; Ye, Y.; Lin, Y.; Yao, X.; Thorne, J.; Liu, E.; McMahon, G.; Zhu, J.; Javey, A.; et al. Enabling unassisted solar water splitting by iron oxide and silicon. *Nat. Commun.* **2015**, *6*, 7447.
(21) Zhang, J.; Eslava, S. Understanding charge transfer, defects and surface states at hematite photoanodes. *Sustain. Energy Fuels* **2019**, *3*, 1351−1364.
(22) Deng, J.; Zhong, J.; Pu, A.; Zhang, D.; Li, M.; Sun, X.; Lee, S.-T. Ti-doped hematite nanostructures for solar water splitting with high efficiency. *J. Appl. Phys.* **2012**, *112*, 084312.
(23) Pu, A.; Deng, J.; Li, M.; Gao, J.; Zhang, H.; Hao, Y.; Zhong, J.; Sun, X. Coupling Ti-doping and oxygen vacancies in hematite nanostructures for solar water oxidation with high efficiency. *J. Mater. Chem. A* **2014**, *2*, 2491−2497.
(24) Klahr, B.; Gimenez, S.; Fabregat-Santiago, F.; Bisquert, J.; Hamann, T. W. Electrochemical and photoelectrochemical investigation of water oxidation with hematite electrodes. *Energy Environ. Sci.* **2012**, *5*, 7626−7636.
(25) Bertoluzzi, L.; Bisquert, J. Equivalent circuit of electrons and holes in thin semiconductor films for photoelectrochemical water splitting applications. *J. Phys. Chem. Lett.* **2012**, *3*, 2517−2522.
(26) Prévot, M. S.; Jeanbourquin, X. A.; Bourée, W. S.; Abdi, F.; Friedrich, D.; Van De Krol, R.; Guijarro, N.; Le Formal, F.; Sivula, K. Evaluating charge carrier transport and surface states in $CuFeO_2$ photocathodes. *Chem. Mater.* **2017**, *29*, 4952−4962.
(27) Dotan, H.; Sivula, K.; Grätzel, M.; Rothschild, A.; Warren, S. C. Probing the photoelectrochemical properties of hematite (α-Fe_2O_3) electrodes using hydrogen peroxide as a hole scavenger. *Energy Environ. Sci.* **2011**, *4*, 958−964.
(28) Sivula, K.; Le Formal, F.; Grätzel, M. Solar water splitting: progress using hematite (α-Fe_2O_3) photoelectrodes. *ChemSusChem* **2011**, *4*, 432−449.
(29) Sivula, K.; Zboril, R.; Le Formal, F.; Robert, R.; Weidenkaff, A.; Tucek, J.; Frydrych, J.; Gratzel, M. Photoelectrochemical water splitting with mesoporous hematite prepared by a solution-based colloidal approach. *J. Am. Chem. Soc.* **2010**, *132*, 7436−7444.
(30) Lin, Y.; Yuan, G.; Sheehan, S.; Zhou, S.; Wang, D. Hematite-based solar water splitting: challenges and opportunities. *Energy Environ. Sci.* **2011**, *4*, 4862−4869.
(31) Zandi, O.; Hamann, T. W. Enhanced water splitting efficiency through selective surface state removal. *J. Phys. Chem. Lett.* **2014**, *5*, 1522−1526.
(32) Wheeler, D. A.; Wang, G.; Ling, Y.; Li, Y.; Zhang, J. Z. Nanostructured hematite: synthesis, characterization, charge carrier dynamics, and photoelectrochemical properties. *Energy Environ. Sci.* **2012**, *5*, 6682−6702.
(33) van de Krol, R.; Grätzel, M. *Photoelectrochemical Hydrogen Production*; Electronic Materials: Science & Technology; Springer Science+Business Media: New York, 2011.
(34) Steier, L.; Herraiz-Cardona, I.; Gimenez, S.; Fabregat-Santiago, F.; Bisquert, J.; Tilley, S. D.; Grätzel, M. Understanding the role of underlayers and overlayers in thin film hematite photoanodes. *Adv. Funct. Mater.* **2014**, *24*, 7681−7688.
(35) Klahr, B.; Hamann, T. Water oxidation on hematite photoelectrodes: insight into the nature of surface states through in situ spectroelectrochemistry. *J. Phys. Chem. C* **2014**, *118*, 10393−10399.
(36) Pendlebury, S. R.; Barroso, M.; Cowan, A. J.; Sivula, K.; Tang, J.; Grätzel, M.; Klug, D.; Durrant, J. R. Dynamics of photogenerated holes in nanocrystalline α-Fe_2O_3 electrodes for water oxidation

https://dx.doi.org/10.1021/acs.jpcc.0c00798
J. Phys. Chem. C 2020, 124, 13094−13101

probed by transient absorption spectroscopy. *Chem. Commun.* **2011**, *47*, 716−718.
(37) Ruoko, T.-P.; Kaunisto, K.; Bärtsch, M.; Pohjola, J.; Hiltunen, A.; Niederberger, M.; Tkachenko, N. V.; Lemmetyinen, H. Subpicosecond to second time-scale charge carrier kinetics in hematite-titania nanocomposite photoanodes. *J. Phys. Chem. Lett.* **2015**, *6*, 2859−2864.
(38) Pei, G. X.; Wijten, J. H.; Weckhuysen, B. M. Probing the dynamics of photogenerated holes in doped hematite photoanodes for solar water splitting using transient absorption spectroscopy. *Phys. Chem. Chem. Phys.* **2018**, *20*, 9806−9811.
(39) Pendlebury, S. R.; Wang, X.; Le Formal, F.; Cornuz, M.; Kafizas, A.; Tilley, S. D.; Grätzel, M.; Durrant, J. R. Ultrafast charge carrier recombination and trapping in hematite photoanodes under applied bias. *J. Am. Chem. Soc.* **2014**, *136*, 9854−9857.

https://dx.doi.org/10.1021/acs.jpcc.0c00798
J. Phys. Chem. C 2020, 124, 13094−13101